Journal of Zhejiang University-SCIENCE A (Applied Physics & Engineering)
ISSN 1673-565X (Print); ISSN 1862-1775 (Online)
www.jzus.zju.edu.cn; link.springer.com
E-mail: jzus_a@zju.edu.cn

Carbon self-doped polytriazine imide nanotubes with optimized electronic structure for enhanced photocatalytic activity*#

Hui ZHANG, Zhen YANG, Yu-qi CAO, Zhi-gang MOU, Xin CAO†‡, Jian-hua SUN†‡

School of Chemistry and Environmental Engineering, Institute of Advanced Functional Materials for Energy, Jiangsu University of Technology, Changzhou 213001, China

†E-mail: caoxin@jsut.edu.cn; sunjh@jsut.edu.cn

Received Aug. 26, 2020; Revision accepted Jan. 11, 2021; Crosschecked Aug. 26, 2021

Abstract: The triazine-based carbon nitride known as polytriazine imide (PTI) is a metal-free semiconductor photocatalyst but usually shows moderate activity due to its limited charge transfer mobility. Here, carbon self-doped PTI (C-PTI) was prepared via a facile and green method by using glucose as the carbon source. In the condensation process, glucose can promote nanotube formation, giving the product larger surface areas. Moreover, carbon self-doping induces an intrinsic change in the electronic structure, thus optimizing the band structure and the electronic transport property. Therefore, the as-synthesized C-PTI exhibits remarkably enhanced photocatalytic activities for both hydrogen evolution and tetracycline degradation reactions.

Key words: Polytriazine imide (PTI); Photocatalysis; Hydrogen evolution; Tetracycline degradation
https://doi.org/10.1631/jzus.A2000386 **CLC number:** O643.3

1 Introduction

Photocatalysis has been recognized as a promising strategy to address the global energy shortage and environmental problems; using solar energy can produce clean fuel hydrogen and decompose pollutants (Ong et al., 2016; Huang et al., 2019; Deng et al., 2020). To date, a variety of metal-based oxides, sulfides, and nitrides have been widely studied as photocatalysts to absorb sunlight and generate electron-hole pairs to induce redox reactions (Stolarczyk et al., 2018; Gusain et al., 2019). However, these materials generally have some limitations such as poor visible-light response and/or photocorrosion (Ma et al., 2016; Zhong et al., 2016; Yu et al., 2018; Liu et al., 2019).

In the exploration of efficient and stable photocatalysts, a polymeric semiconductor known as carbon nitride (CN), with excellent chemical stability and suitable band structure, has exhibited outstanding performance in the field of solar energy utilization (Wang XC et al., 2009; Liu et al., 2015; Zhao et al., 2015; Wang XL et al., 2018). The CN synthesized by traditional thermal condensation of nitrogen-rich precursors is known as a N-bridged "poly(tri-*s*-triazine)" (Wang et al., 2012). Due to the layered structure similar to graphene, it is usually called graphitic carbon nitride (g-C_3N_4). In recent years, molten salt methods have been developed for the synthesis of CNs. Previous studies indicate that the use of salt melts causes CN building blocks to convert from tri-*s*-triazine to *s*-triazine (Wirnhier et al., 2011; Schwinghammer et al., 2013; Heymann et al., 2018; Jia et al., 2018). The as-prepared CN is often named polytriazine imide (PTI).

‡ Corresponding author

* Project supported by the National Natural Science Foundation of China (No. 51702134), the Natural Science Foundation of Jiangsu Province (No. BK20170310), the PhD Research Startup Foundation of Jiangsu University of Technology (No. KYY18038), and the Postgraduate Research & Practice Innovation Program of Jiangsu Province (No. XSJCX20_01), China

Electronic supplementary materials: The online version of this article (https://doi.org/10.1631/jzus.A2000386) contains supplementary materials, which are available to authorized users

ORCID: Hui ZHANG, https://orcid.org/0000-0002-0591-2098

Compared to traditional condensation, the molten salt method has advantages in controlling product morphology, thus often resulting in a larger surface area and shorter photocarrier migration distance. However, pristine PTI still exhibits moderate photocatalytic activity (Ham et al., 2013; Zhang H et al., 2016). A major reason might be that its reduced conjugation structure leads to limited charge transfer mobility (Lin et al., 2016). To address the problem, it is imperative to modulate the electronic structure and charge transport properties.

It is well known that the self-doping method can tune the surface properties and electronic structure of a semiconductor photocatalyst without introducing foreign impurities as recombination centers (Zuo et al., 2010; Fang et al., 2015; Wei et al., 2018). In particular, carbon self-doping can increase electrical conductivity and thus accelerate charge transfer (Dong et al., 2012). In this study, we developed a facile method to prepare carbon self-doped PTI (C-PTI) by thermal polymerization of melamine and glucose in LiCl/KCl salt melts. During the synthesis, no toxic precursors or organic solvents were used. Our study demonstrated that the incorporation of the carbon source, glucose, can promote nanotube formation during condensation, thus giving the product larger surface areas. Moreover, carbon self-doping induces an intrinsic change in the electronic structure, thus optimizing the band structure and the electronic transport property. Therefore, the as-synthesized C-PTI exhibits enhanced photocatalytic activities for both reduction and oxidation reactions with respect to those of pure PTI.

2 Experimental

2.1 Synthesis procedure

For the synthesis of C-PTI, a thoroughly grounded mixture of melamine (1.00 g), glucose (0.004 g), LiCl (4.50 g), and KCl (5.50 g) was heated in a muffle furnace at 550 °C for 4 h. The heating rate was 2.1 °C/min. After cooling to room temperature, the obtained mixture was dispersed in water and stirred at 90 °C for 0.5 h. Then the gray solid was collected by filtration, washed with water, and dried at 60 °C. The light yellow pure PTI was prepared following the above procedure without the use of glucose.

g-C_3N_4 was synthesized by thermal condensation of melamine: 2.00-g melamine was heated in a muffle furnace at 550 °C for 4 h. The obtained solid was thoroughly grounded and collected as the product.

2.2 Hydrogen evolution experiments

Photocatalytic hydrogen production experiments were performed in a sealed top-irradiation reaction vessel. Typically, a 50-mg sample was dispersed in a mixture of 90-mL deionized water and 10-mL triethanolamine (TEOA). After addition of 3% (in weight) H_2PtCl_6 (based on Pt), the system was degassed and then irradiated under a 300-W Xe lamp with a 420-nm cut-off filter. During the reaction, the suspension was stirred at 20 °C, controlled by cycle water. The gas product was analyzed by on-line gas chromatography, using argon as the carrier gas.

2.3 Tetracycline degradation experiments

Photocatalytic tetracycline degradation experiments were carried out in a top-irradiation reaction vessel and the reaction temperature was 20 °C, controlled by cycle water. A 300-W Xe lamp with a 420-nm cut-off filter was used as the light source. In a typical procedure, a 50-mg sample was dispersed in 100 mL of 30-mg/L tetracycline aqueous solution and was stirred in the dark for 40 min prior to irradiation. During the reaction, 4 mL of the suspension fluid was collected from the reaction vessel every 20 min and filtered through a 0.45-μm filter to remove the photocatalysts. The resulting solution was analyzed by a UV1800PC spectrophotometer (USA) at a wavelength of 358 nm. The active species trapping experiments were conducted by adding a corresponding scavenger (1.0 mmol) or by removal of O_2: isopropanol (IPA) and disodium ethylenediaminetetraacetate (EDTA-2Na) were selected as the scavengers of ·OH and h^+, respectively. For the elimination of $\cdot O_2^-$, the reaction system was evacuated and then filled with N_2 several times to completely remove O_2.

3 Results and discussion

Carbon doping levels could be controlled by tuning the amount of glucose added, as described in the electronic supplementary materials (ESM). We took the optimized C-PTI sample as an example to

demonstrate that carbon self-doping gave rise to certain changes in the morphological properties, band structures, charge transport properties, and photocatalytic activities.

The structures of the as-prepared samples were confirmed by X-ray diffraction (XRD) (PW3040/60P analytical X'Pert PRO diffractometer, the Netherlands) and Fourier transform infrared (FT-IR) (Thermo Nicolet iS10 spectrometer, USA). As shown in Fig. 1a, the XRD pattern of PTI was consistent with previous studies (Wirnhier et al., 2011; Zhang YL et al., 2016). The strongest peak at 26.6° corresponded to the (002) plane of PTI. We ascribed this peak to the stacking of conjugated aromatic rings, with an interlayer distance of 0.335 nm. The C-PTI sample exhibited similar diffraction peaks to those of PTI. Somewhat differently, as displayed in Fig. 1b, the (002) peak of C-PTI shifted to 26.4°, with an increased distance of 0.337 nm. This crystal distortion might have arisen from carbon doping in PTI. Fig. S4 in ESM presents the FT-IR spectra of PTI and

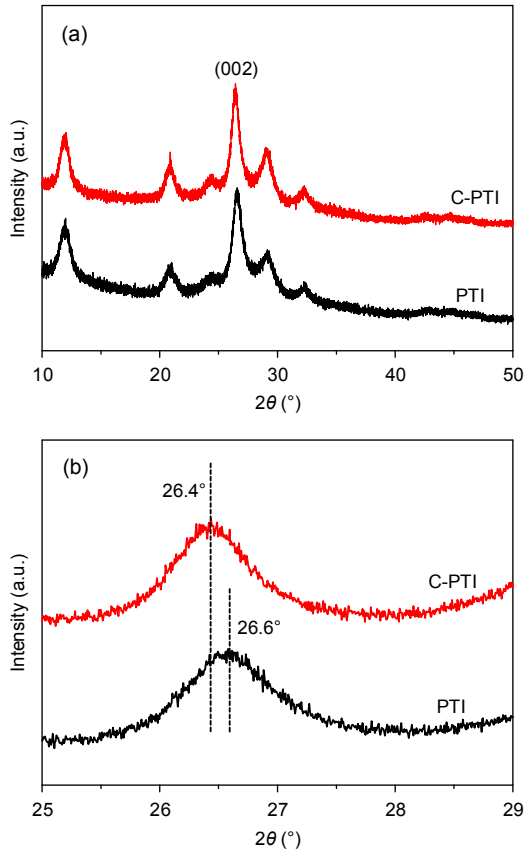

Fig. 1 XRD patterns of PTI (a) and C-PTI (b)

C-PTI. Both spectra contained characteristic peaks assigned to vibrational modes in PTI. In detail, several strong bands at 1200–1650 cm^{-1} were attributable to the stretching modes of C-N and C=N in the triazine rings. The sharp peaks at 806 cm^{-1} originated from the out-of-plane bending vibrations of triazine units (Schwinghammer et al., 2013). We attributed the broad bands at 3000−3500 cm^{-1} to N-H stretching (Bojdys et al., 2008; Suter et al., 2019).

The high-resolution X-ray photoelectron spectroscopy (XPS) (VG Multilab 2000 X-ray photoelectron spectrometer, USA) spectra of C 1s for PTI and C-PTI in Fig. 2a could be deconvoluted into three peaks at 284.7, 285.9, and 288.2 eV. The peak at 284.7 eV is regarded as adventitious carbon (especially graphitic C=C and grease), while the peaks at 285.9 and 288.2 eV are assigned to the sp^2 C bonded to N in the triazine ring (Schwinghammer et al., 2014). Interestingly, the percentage of the peak at 284.7 eV increased from 31.5% to 33.6% for C-PTI compared to PTI, which may be caused by carbon doping in the C-PTI sample. Fig. 2b is the spectra of N 1s for the two samples. Two major peaks were identified at 398.7 and 400.3 eV, which can be ascribed to the N atoms in triazine units and the bridging N atoms in NH groups, respectively (Schwinghammer et al., 2014; Zhang et al., 2019). Also, the decreased percentage of the peak at 400.3 eV for C-PTI (23.9%) with respect to PTI (24.3%) suggests the probable replacement of bridging N with C due to carbon self-doping.

The morphological properties of the synthesized samples were investigated by scanning electron microscopy (SEM) and transmission electron microscopy (TEM). SEM and TEM images were collected on a Hitachi S-3400N microscopy and an JEM-2100 instrument (Japan), respectively. As shown in Figs. 3a and 3c, PTI presents a typical cracked nanotube structure. When the carbon source glucose was introduced into the precursor, the obvious hollow nanotubes formed in C-PTI, as shown in Figs. 3b and 3d. The change in morphology may be due to the hydrogen bonds between glucose and melamine; these bonds enhance the toughness of PTI to suppress the destruction of bubbles induced by released gases during the pyrolysis process (Wang Y et al., 2018). Moreover, the morphology change results in a larger special surface area for C-PTI than that of PTI (about

174 m^2/g vs. 157 m^2/g), as determined from the N_2 adsorption-desorption isotherm (Fig. S6). Therefore, C-PTI can provide more reaction sites and would be more active in photocatalytic reactions.

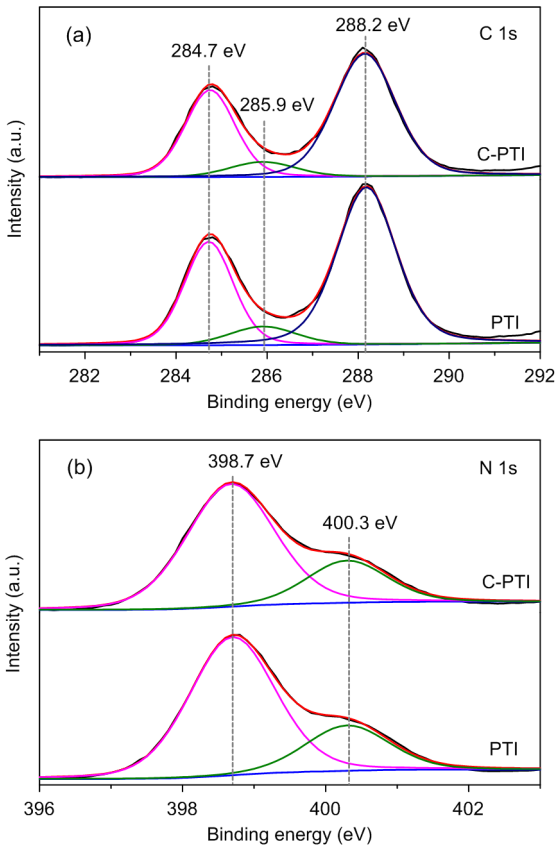

Fig. 2 High-resolution XPS spectra of C 1s (a) and N 1s (b) for PTI and C-PTI

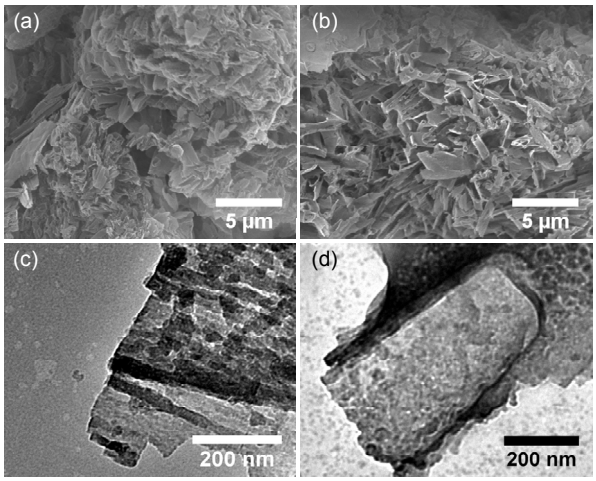

Fig. 3 SEM images of PTI (a) and C-PTI (b); TEM images of PTI (c) and C-PTI (d)

The photocatalytic performance of a semiconductor is closely related to its band-gap position. To identify the band structures of the prepared samples, the UV-vis diffuse reflection spectra (DRS), Mott-Schottky plots, and valence band (VB) XPS spectra were measured. Fig. 4a shows the UV-vis DRS of PTI and C-PTI. The absorption edges were around 450 nm, and there were extended visible-light absorptions over 450−800 nm for both of them, which enabled the possible utilization of visible light. The band gaps (E) could be estimated by the corresponding Tauc plots. As illuminated in the insert, the band gap of C-PTI was 3.05 eV, slightly wider than that of pristine PTI (2.96 eV). Meanwhile, the Mott-Schottky plots in Fig. 4b indicate that the conduction bands (CBs) of PTI and C-PTI were determined to be −0.57 V and −0.60 V (vs. normal hydrogen electrode (NHE), pH=7), respectively. Furthermore, as observed from Fig. 4c, C-PTI displayed a VB shift of 0.07 V, in line with the calculated results obtained from the band gaps and CBs. Based on the above results, the band structures of the two samples can be resolved in Fig. 4d, which clearly demonstrates that both of the samples can thermodynamically enable photocatalytic H_2 evolution and $\cdot O_2^-$ production reactions. More importantly, the more negative CB and positive VB of C-PTI compared to those of PTI result in higher redox abilities. As a consequence, C-PTI could be more favorable for photocatalytic redox reactions.

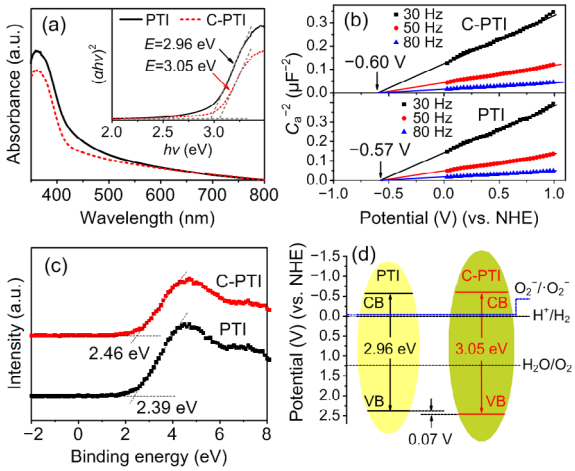

Fig. 4 UV-vis DRS and the corresponding Tauc plots (insert) (a), Mott-Schottky plots (b), VB XPS spectra (c), and band structure alignments of PTI and C-PTI (d)

h is Planck's constant, ν is the frequency of the incident light, and C_a is the capacitance

The photogenerated charge carrier transfer also plays a crucial role in photocatalytic reactions. To study the charge-transfer resistances of the resulting samples, we measured electrochemical impedance spectra (EIS); the results are displayed in Fig. 5. The Nyquist plot diameter of C-PTI was smaller than that of PTI, indicating an increased electrical conductivity of C-PTI caused by carbon self-doping. Benefitting from the increased charge mobility, C-PTI could more efficiently restrain the photogenerated electron-hole recombination. This can be verified by the enhanced photocurrent density in Fig. 5b and reduced fluorescence intensity in Fig. S7.

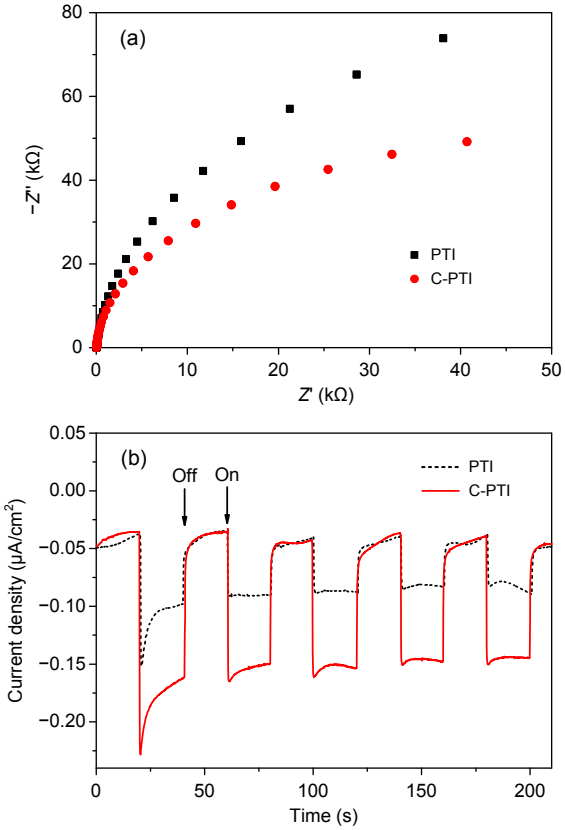

Fig. 5 EIS plots (a) and transient photocurrent responses (b) of PTI and C-PTI

Z' and Z'' are the real and imaginary parts of the complex impedance, respectively

The photocatalytic performance of the as-synthesized samples was first investigated by hydrogen production reactions under visible light irradiation. The H_2-evolving water-splitting half reactions were carried out in a TEOA aqueous solution. As demonstrated in Fig. 6a, the PTI sample showed poor photoreduction performance, with a hydrogen evolution rate of 0.82 μmol/h; this could be caused by the limited charge transfer mobility and the fast charge carrier recombination. The even lower H_2 evolution rate in the first hour is due to the insufficient reduction of the platinum cations. C-PTI presented significantly enhanced photocatalytic H_2 production activity (4.6 μmol/h), about 5.6 times higher than that of PTI. Thus, we concluded that carbon self-doping can induce significantly increased photoreduction activity of PTI. In addition, the C-PTI sample maintained its photocatalytic activity after 12-h irradiation with visible light (Fig. 6b), which indicates good stability of the photocatalyst.

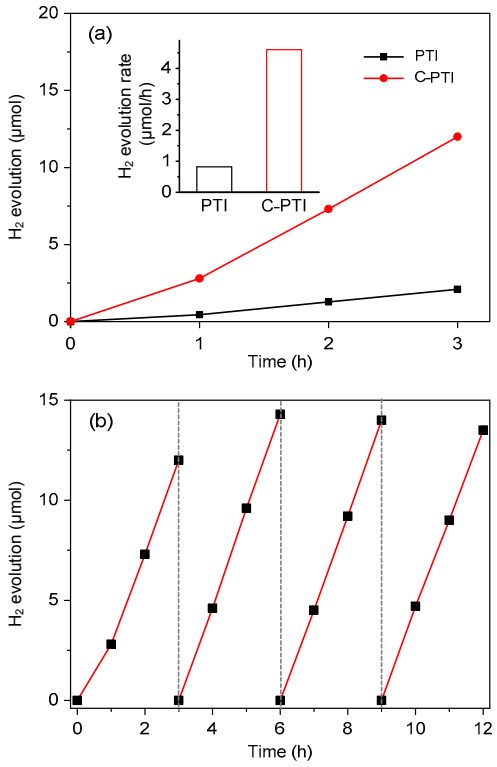

Fig. 6 H_2 evolution of PTI and C-PTI under visible light irradiation (a) and time course of photocatalytic H_2 evolution activity of C-PTI (b)

The photocatalytic oxidation activity of the samples was further evaluated by tetracycline degradation reactions under visible light irradiation. To demonstrate the perfect photocatalytic oxidation performance of C-PTI, we also compared its degradation efficiency with that of g-C_3N_4 (Brunner-Emmet-Teller surface area S_{BET}=11.7 m^2/g), which was synthesized by traditional condensation of

melamine. As shown in Fig. 7a, the removal of tetracycline was 20% by g-C_3N_4 after 60 min irradiation. For the PTI photocatalyst, the tetracycline degradation efficiency was significantly increased to 70%. This increment may be caused by a higher photooxidation ability of PTI, which arises from much more positive VB (2.39 V vs. NHE, Figs. 4c and 4d) of PTI compared to that of g-C_3N_4 (1.57 V vs. NHE) (Wang et al., 2009). Meanwhile, an even higher tetracycline degradation efficiency (up to 79%) was achieved by C-PTI under the same conditions. The kinetic curves for the tetracycline photocatalytic degradation are presented in Fig. 7b. The removal rate constant k of C-PTI was 0.022 min^{-1}, about 23 times higher than that of g-C_3N_4 (0.00097 min^{-1}), and 1.3 times higher than that of PTI (0.017 min^{-1}). These results indicate a remarkably enhanced photocatalytic oxidation activity of C-PTI.

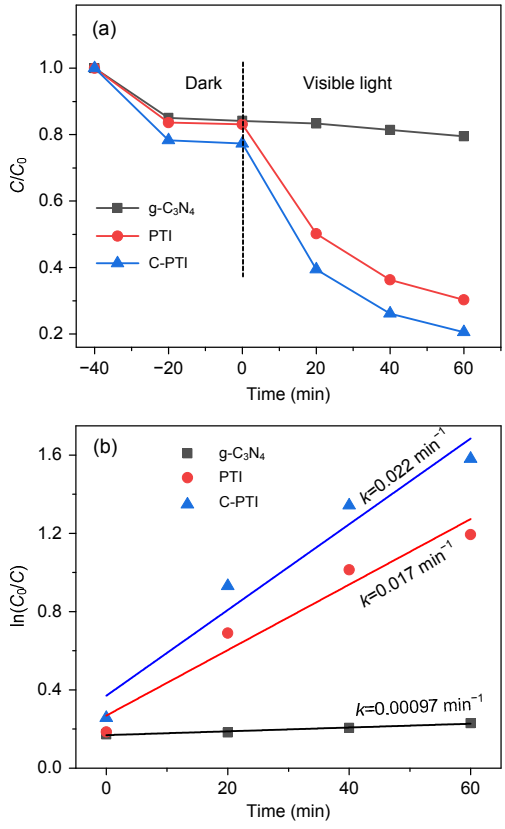

Fig. 7 Dynamic curves (a) and plots of ln(C_0/C) (b) versus time of the photodegradation tetracycline solution over g-C_3N_4, pristine PTI, and C-PTI under visible-light irradiation

C_0 is the initial tetracycline concentration and C is the tetracycline concentration at a given time

In order to check the fate of catalysts for practical applications, we studied the recyclability of C-PTI by adding the same concentration of tetracycline after each reaction cycle without separating the photocatalyst. Fig. S8 shows that photocatalytic degradation was 79% in the first cycling run, and decreased only a little after four cycles. Moreover, the SEM image and XRD pattern of C-PTI after four degradation reaction cycles (Figs. S9 and S10) indicate that there were negligible changes of morphology and crystal structure in C-PTI. Therefore, the C-PTI photocatalyst has good stability and recyclability.

During the photocatalytic degradation process, the tetracycline was adsorbed on the surface of photocatalysts and could be oxidized by active species such as ·OH, h^+, and $\cdot O_2^-$. To determine the main active species involved in the photocatalytic degradation of tetracycline over C-PTI, active species trapping experiments were carried out. IPA and EDTA-2Na were used as the scavengers of ·OH and h^+, respectively (Mou et al., 2019). The $\cdot O_2^-$ was eliminated by completely replacing O_2 with N_2 in the system (Rimoldi et al., 2019). As shown in Fig. 8, EDTA-2Na and N_2 obviously inhibited tetracycline degradation, which suggests that h^+ and $\cdot O_2^-$ are the two main active species.

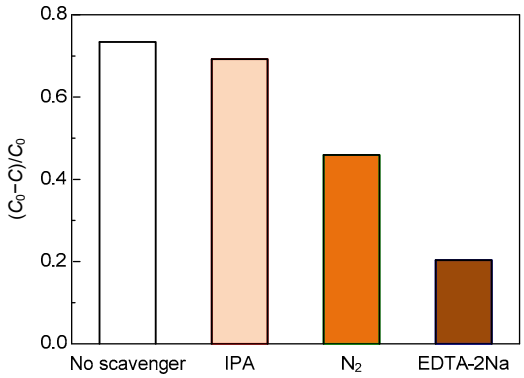

Fig. 8 Photodegradation of tetracycline over C-PTI under visible light (wavelength λ≥420 nm) irradiation with radical scavengers or N_2

Based on the above characterization and discussion, a probable photocatalytic mechanism is presented in Fig. 9. Under visible light irradiation, the photocatalyst generates electron and hole pairs. Usually, the photogenerated electrons and holes are easy to recombine when migrating from the excitation sites to the reaction sites, leading to a low

photocatalytic activity of pristine PTI. However, carbon self-doping induces increased electrical conductivity (Fig. 5) and contributes to fast charge transfer. Therefore, an obvious suppression of photocarrier recombination was observed in C-PTI (Figs. 5b and S7). Moreover, the negative shift of CB and positive shift of VB (Fig. 4d) result in higher reduction and oxidation ability of C-PTI, respectively. As a result, the as-synthesized C-PTI exhibits enhanced photocatalytic activity in both H_2 evolution and tetracycline degradation reactions.

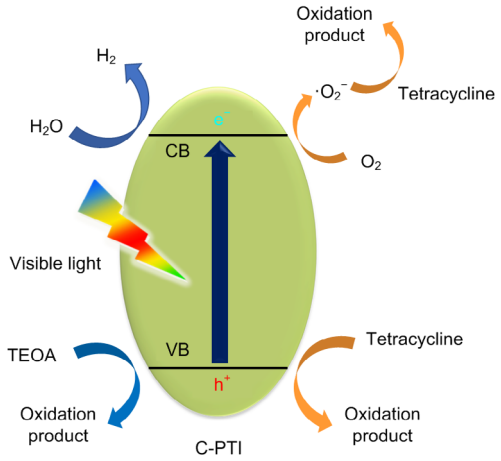

Fig. 9 Proposed photocatalytic mechanism of H_2 evolution and tetracycline degradation by C-PTI

4 Conclusions

In summary, we have successfully synthesized carbon self-doped PTI photocatalysts via a facile and green method by using glucose as the carbon source. Carbon self-doping induces a large surface area, negative shift of CB, positive shift of VB, and increased charge transfer mobility. These changes result in remarkably enhanced photocatalytic activities for both hydrogen evolution and tetracycline degradation reactions. This work provides a novel strategy to optimize the electronic structures as well as the surface properties of PTI in order to improve photocatalytic performance.

Contributors

Hui ZHANG designed the research. Hui ZHANG, Zhen YANG, Yu-qi CAO, and Zhi-gang MOU processed the corresponding data. Hui ZHANG wrote the first draft of the manuscript. Xin CAO and Jian-hua SUN helped to organize the manuscript. Hui ZHANG revised and edited the final version.

Conflict of interest

Hui ZHANG, Zhen YANG, Yu-qi CAO, Zhi-gang MOU, Xin CAO, and Jian-hua SUN declare that they have no conflict of interest.

References

Bojdys MJ, Müller JO, Antonietti M, et al., 2008. Ionothermal synthesis of crystalline, condensed, graphitic carbon nitride. *Chemistry-A European Journal*, 14(27):8177-8182. https://doi.org/10.1002/chem.200800190

Deng YC, Li ZY, Tang RD, et al., 2020. What will happen when microorganisms "meet" photocatalysts and photocatalysis? *Environmental Science: Nano*, 7(3):702-723. https://doi.org/10.1039/c9en01318k

Dong GH, Zhao K, Zhang LZ, 2012. Carbon self-doping induced high electronic conductivity and photoreactivity of g-C_3N_4. *Chemical Communications*, 48(49):6178-6180. https://doi.org/10.1039/C2CC32181E

Fang JW, Fan HQ, Li MM, et al., 2015. Nitrogen self-doped graphitic carbon nitride as efficient visible light photocatalyst for hydrogen evolution. *Journal of Materials Chemistry A*, 3(26):13819-13826. https://doi.org/10.1039/C5TA02257F

Gusain R, Gupta K, Joshi P, et al., 2019. Adsorptive removal and photocatalytic degradation of organic pollutants using metal oxides and their composites: a comprehensive review. *Advances in Colloid and Interface Science*, 272:102009. https://doi.org/10.1016/j.cis.2019.102009

Ham Y, Maeda K, Cha D, et al., 2013. Synthesis and photocatalytic activity of poly (triazine imide). *Chemistry–An Asian Journal*, 8(1):218-224. https://doi.org/10.1002/asia.201200781

Heymann L, Bittinger SC, Klinke C, 2018. Molecular doping of electrochemically prepared triazine-based carbon nitride by 2,4,6-triaminopyrimidine for improved photocatalytic properties. *ACS Omega*, 3(12):17042-17048. https://doi.org/10.1021/acsomega.8b02659

Huang DL, Chen S, Zeng GM, et al., 2019. Artificial Z-scheme photocatalytic system: what have been done and where to go? *Coordination Chemistry Reviews*, 385:44-80. https://doi.org/10.1016/j.ccr.2018.12.013

Jia JJ, White ER, Clancy AJ, et al., 2018. Fast exfoliation and functionalisation of two-dimensional crystalline carbon nitride by framework charging. *Angewandte Chemie International Edition*, 57(39):12656-12660. https://doi.org/10.1002/anie.201800875

Lin LH, Ou HH, Zhang YF, et al., 2016. Tri-*s*-triazine-based crystalline graphitic carbon nitrides for highly efficient hydrogen evolution photocatalysis. *ACS Catalysis*, 6(6):3921-3931.

https://doi.org/10.1021/acscatal.6b00922

Liu BS, Yang JJ, Wang JY, et al., 2019. High sub-band gap response of TiO_2 nanorod arrays for visible photoelectrochemical water oxidation. *Applied Surface Science*, 465:192-200. https://doi.org/10.1016/j.apsusc.2018.09.098

Liu J, Liu Y, Liu NY, et al., 2015. Metal-free efficient photocatalyst for stable visible water splitting via a two-electron pathway. *Science*, 347(6225):970-974. https://doi.org/10.1126/science.aaa3145

Ma FK, Wu YZ, Shao YL, et al., 2016. 0D/2D nanocomposite visible light photocatalyst for highly stable and efficient hydrogen generation via recrystallization of CdS on MoS_2 nanosheets. *Nano Energy*, 27:466-474. https://doi.org/10.1016/j.nanoen.2016.07.014

Mou ZG, Zhang H, Liu ZM, et al., 2019. Ultrathin BiOCl/nitrogen-doped graphene quantum dots composites with strong adsorption and effective photocatalytic activity for the degradation of antibiotic ciprofloxacin. *Applied Surface Science*, 496:143655. https://doi.org/10.1016/j.apsusc.2019.143655

Ong WJ, Tan LL, Ng YH, et al., 2016. Graphitic carbon nitride ($g\text{-}C_3N_4$)-based photocatalysts for artificial photosynthesis and environmental remediation: are we a step closer to achieving sustainability? *Chemical Reviews*, 116(12):7159-7329. https://doi.org/10.1021/acs.chemrev.6b00075

Rimoldi L, Giordana A, Cerrato G, et al., 2019. Insights on the photocatalytic degradation processes supported by TiO_2/WO_3 systems. The case of ethanol and tetracycline. *Catalysis Today*, 328:210-215. https://doi.org/10.1016/j.cattod.2018.11.035

Schwinghammer K, Tuffy B, Mesch MB, et al., 2013. Triazine-based carbon nitrides for visible-light-driven hydrogen evolution. *Angewandte Chemie International Edition*, 52(9):2435-2439. https://doi.org/10.1002/anie.201206817

Schwinghammer K, Mesch MB, Duppel V, et al., 2014. Crystalline carbon nitride nanosheets for improved visible-light hydrogen evolution. *Journal of the American Chemical Society*, 136(5):1730-1733. https://doi.org/10.1021/ja411321s

Stolarczyk JK, Bhattacharyya S, Polavarapu L, et al., 2018. Challenges and prospects in solar water splitting and CO_2 reduction with inorganic and hybrid nanostructures. *ACS Catalysis*, 8(4):3602-3635. https://doi.org/10.1021/acscatal.8b00791

Suter TM, Miller TS, Cockcroft JK, et al., 2019. Formation of an ion-free crystalline carbon nitride and its reversible intercalation with ionic species and molecular water. *Chemical Science*, 10(8):2519-2528. https://doi.org/10.1039/C8SC05232H

Wang XC, Maeda K, Thomas A, et al., 2009. A metal-free polymeric photocatalyst for hydrogen production from water under visible light. *Nature Materials*, 8(1):76-80. https://doi.org/10.1038/nmat2317

Wang XL, Liu Q, Yang Q, et al., 2018. Three-dimensional $g\text{-}C_3N_4$ aggregates of hollow bubbles with high photocatalytic degradation of tetracycline. *Carbon*, 136:103-112. https://doi.org/10.1016/j.carbon.2018.04.059

Wang Y, Wang XC, Antonietti M, 2012. Polymeric graphitic carbon nitride as a heterogeneous organocatalyst: from photochemistry to multipurpose catalysis to sustainable chemistry. *Angewandte Chemie International Edition*, 51(1):68-89. https://doi.org/10.1002/anie.201101182

Wang Y, Liu XQ, Liu J, et al., 2018. Carbon quantum dot implanted graphite carbon nitride nanotubes: excellent charge separation and enhanced photocatalytic hydrogen evolution. *Angewandte Chemie International Edition*, 57(20):5765-5771. https://doi.org/10.1002/anie.201802014

Wei FY, Liu Y, Zhao H, et al., 2018. Oxygen self-doped $g\text{-}C_3N_4$ with tunable electronic band structure for unprecedentedly enhanced photocatalytic performance. *Nanoscale*, 10(9):4515-4522. https://doi.org/10.1039/C7NR09660G

Wirnhier E, Döblinger M, Gunzelmann D, et al., 2011. Poly(triazine imide) with intercalation of lithium and chloride ions $[(C_3N_3)_2(NH_xLi_{1-x})_3\cdot LiCl]$: a crystalline 2D carbon nitride network. *Chemistry–A European Journal*, 17(11):3213-3221. https://doi.org/10.1002/chem.201002462

Yu YG, Yang X, Zhao YL, et al., 2018. Engineering the band gap states of the rutile $TiO_2(110)$ surface by modulating the active heteroatom. *Angewandte Chemie-International Edition*, 57(28):8550-8554. https://doi.org/10.1002/anie.201803928

Zhang H, Liu F, Mou ZG, et al., 2016. A facile one-step synthesis of ZnO quantum dots modified poly(triazine imide) nanosheets for enhanced hydrogen evolution under visible light. *Chemical Communications*, 52(88):13020-13023. https://doi.org/10.1039/C6CC06970C

Zhang H, Cao YQ, Zhong L, et al., 2019. Fast photogenerated electron transfer in N-GQDs/PTI/ZnO-QDs ternary heterostructured nanosheets for photocatalytic H_2 evolution under visible light. *Applied Surface Science*, 485:361-367. https://doi.org/10.1016/j.apsusc.2019.04.230

Zhang YL, Hu LL, Zhu C, et al., 2016. Air activation by a metal-free photocatalyst for "totally-green" hydrocarbon selective oxidation. *Catalysis Science & Technology*, 6(19):7252-7258. https://doi.org/10.1039/C6CY01066K

Zhao ZW, Sun YJ, Dong F, 2015. Graphitic carbon nitride based nanocomposites: a review. *Nanoscale*, 7(1):15-37. https://doi.org/10.1039/c4nr03008g

Zhong YY, Zhao G, Ma FK, et al., 2016. Utilizing photocorrosion-recrystallization to prepare a highly stable and efficient CdS/WS_2 nanocomposite photocatalyst for

hydrogen evolution. *Applied Catalysis B: Environmental*, 199:466-472. https://doi.org/10.1016/j.apcatb.2016.06.065

Zuo F, Wang L, Wu T, et al., 2010. Self-doped Ti^{3+} enhanced photocatalyst for hydrogen production under visible light. *Journal of the American Chemical Society*, 132(34): 11856-11857. https://doi.org/10.1021/ja103843d

List of electronic supplementary materials

Data S1 Characterization

Data S2 Photoelectrochemical measurements

Data S3 Synthesis of carbon doped PTI with various carbon doping levels

Data S4 Characterization, optical properties, and photocatalytic H_2 evolution activities of PTI and C_x-PTI